THE HYDROGEOCHEMICAL MODEL OF "YR" GEOTHERMAL FIELD, EAST JAVA

Yunisa Rachmalia[1]*, Agus Didit Haryanto[1], and Johanes Hutabarat[1], and Yuniar Zhafira Abdillah[2]
[1]Faculty of Geological Engineering, Universitas Padjadjaran
[2]PT. Geo Dipa Energi (Persero)
*Corresponding author: yunisa19001@mail.unpad.ac.id

ABSTRACT

The YR Geothermal Field is located in East Java. This field is associated with an active volcano, implying a potential for a high enthalpy geothermal system. This field is still in the exploration phase, but no drilling has been conducted yet. Thus, insights into the geothermal system are obtained through geochemical analyses of geothermal manifestations. Geochemical analyses were performed on hot spring water samples to determine the characteristics, processes, origin, and fluid flow of the geothermal system. The research results indicate that the warm springs have temperatures ranging from 29.4 to 54.8°C, with a nearly neutral pH (6.14-6.44) and high contents of HCO_3 (457-1150 mg/kg), Na (77.7-255 mg/kg), and Mg (37.4-110 mg/kg). Therefore, it can be concluded that all the warm springs fall into the bicarbonate type with immature conditions, indicating no direct association with the reservoir. The upflow zone is interpreted to be at the peak of Mount 7, while the outflow zones are in areas A, B, and C. The fluids flow from the upflow zone, then condense and advectively flow down the slope, experiencing dilution and reactions with rocks before emerging as outflows in the western and north-western areas.

Keyword: Geothermal, YR Field, East Java, geochemistry, warm spring

INTRODUCTION

Young volcanic zones along the convergent plate boundaries are one of the main targets for geothermal energy exploration (Bogie et al., 2005). Indonesia lies within the intersection of four tectonic plates i.e. the Indo-Australian plate, Philippine Sea plate, Caroline plate, and Sunda plate (Hutchings & Mooney, 2021). The convergence between Indo-Australian plate and Sunda plate forming the magmatic arc of the Sunda subduction zone (Simkin & Siebert, 1994), making Indonesia the host of the largest geothermal potential in the world. Among the geothermal potential areas is the YR geothermal field in East Java, characterized by the presence of surface manifestations such as fumaroles and warm springs.

Areas with active volcanoes typically host high-enthalpy hydrothermal systems with drastic geothermal gradients and reach high temperatures only at a shallow depth (Stober & Bucher, 2013). The YR geothermal field is associated with an active volcano, with the last eruption occurring in 1950 (ESDM, 2023). This association suggests the potential presence of a high-enthalpy system within the field. This field is still in the exploration phase, but no drilling has been conducted yet. Therefore, information regarding the conditions of this geothermal system can be obtained through geochemical analysis of geothermal manifestations. This research aims to provide a better understanding of the geothermal system within YR field and remove the uncertainties in future exploration and exploitation phase by developing a hydrogeochemical model.

RESEARCH METHOD

The method used in this study involves geochemical analyses using secondary data. The geochemical fluid data are the results of laboratory analysis from 5 warm spring samples (A1, A2, B, C1, C2), supported by 2 cold spring samples (D1, D2). The chemical water data includes cation (Na, K, Ca, Mg), anion (Cl, SO_4, HCO_3, F, CO_3), neutral elements (B), and stable isotopes (δD and $\delta^{18}O$). In addition to chemical data, other information such as the physical properties of manifestations is also used as supporting data. The available geochemical data were analyzed and interpreted using spreadsheets proposed by Powell and Cumming (2010). Water type and maturity level were identified using Cl-HCO_3-SO_4 (Giggenbach, 1991) and Na-K-Mg (Giggenbach, 1988) diagrams. Cross-plots of δD and $\delta^{18}O$ were employed to determine fluid origin. Fluid processes were determined using Cl-Li-B diagram (Giggenbach, 1991). Finally, various geoindicator ratios were applied to analyze the fluid flow. In this study, pseudonyms was used to replace actual geographical names to ensure the confidentiality and anonymity of specific locations.

E-ISSN : 2579 – 3136

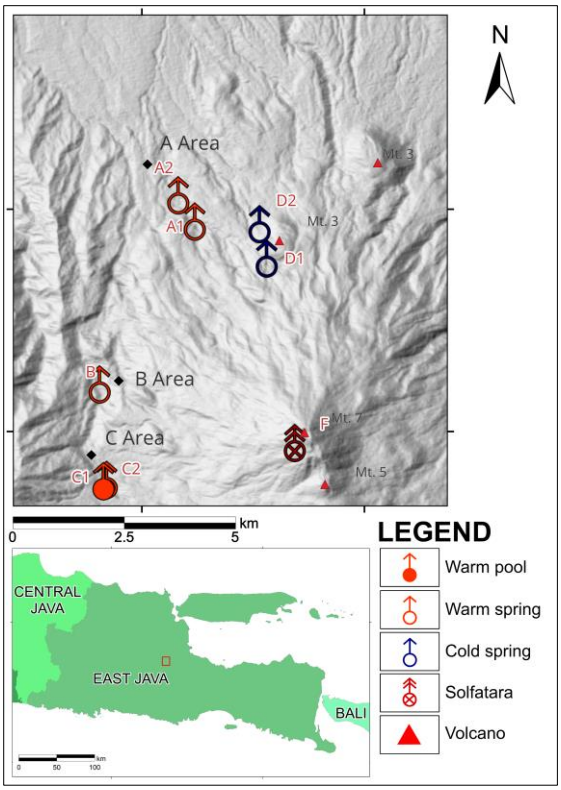

Figure 1. Surface manifestation distribution map showing solfatara (Hadi, 2010) in the peak of Mt. 7, warm springs in the west and northwest flank of Mt. 7, and cold springs located around Mt. 3.

RESULT AND DISCUSSION

General Characteristics

The physical characteristics of the manifestations are presented in Table 1. All warm spring samples have slightly acidic to near-neutral pH values, ranging from 6.14 (A2 to 6.44 (C1 and C2), with temperatures between 29.4-54.8°C. The analysis is also supported by data from cold spring samples with temperatures of 17-25°C and near-neutral to neutral pH values (6.52-7). The Total Dissolved Solids (TDS) values in the hot spring samples range from 854 mg/kg in C2 to 2340 mg/kg in A1, indicating high levels of dissolved constituents. The data also showed the presence of travertine deposits the A2 spring. Chemical contents of the samples from the research area are presented in Table 2, showing high levels of HCO_3 (457-1150 mg/kg), Na (77.7-255 mg/kg), and Mg (37.4-110 mg/kg) in the warm spring samples.

According to Hadi (2010), the volcanic complex associated with YR field exhibits several fumaroles scattered across each peaks. In the research area itself, fumaroles emerge on the peaks of Mt. 7 and Mt. 5. In the peak of Mt. 7, steam emerged forcefully accompanied by sulphur sublimation, forming a solfatara that emits a pungent odor of H_2S gas with a strong hissing sound. The occurrence of the solfatara coincides with an advance argillic alteration zone extending approximately ±1 km^2, and characterized by the presence of alunite, halloysite, and kaolinite mineral assemblages, along with high quantities of iron oxides (Hadi, 2010). Inguaggiato et al. (2018) also conducted sampling in the sulfur-rich fumarole, measuring temperatures reaching up to 220°C. The gas composition is presented in Table 3, displaying high content of water vapor with CO_2, H_2S, and SO_2 as the main constituents of the gas samples.

Water Type

The Cl-HCO_3-SO_4 diagram (Giggenbach, 1991) was used to classify the water types in the geochemical water samples in the research area. Based on their distribution on the diagram (Figure 2), in general, all the warm spring samples can be classified as bicarbonate type. In more detail, the distribution of plots on the diagram is divided into two groups, the first one are the warm springs in area C which plotted at the HCO_3 apex and second one are the warm springs in A and B areas which plotted slightly away from the HCO_3 apex.

Bicarbonate-type water is characterized by low Cl concentrations, relatively high Na concentrations, nearly neutral to alkaline pH, and often accompanied by calcite precipitation (Rahayudin et al., 2020). In volcanic geothermal systems, bicarbonate-rich water is typically produced in peripheral and shallow areas, where CO_2 gas, together with water vapor, underwent a condensation process into groundwater and heated it, resulting in an steam heated HCO_3-rich solution (Nicholson, 1993). Therefore, all the constituents contained in the warm spring water have no direct relation to reservoir fluid.

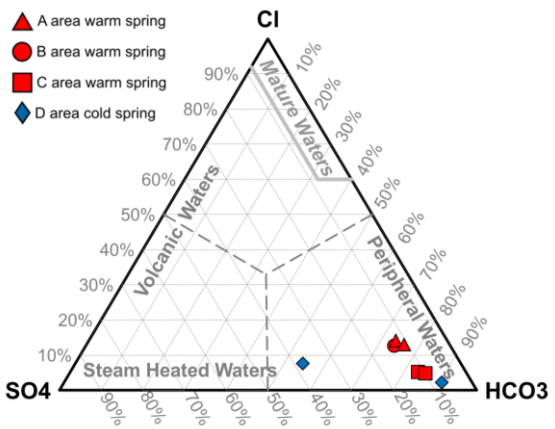

E-ISSN : 2579 – 3136

Figure 2. The Cl-HCO_3-SO_4 diagram (Giggenbach, 1991, cited in Cumming & Powell, 2010) showing that all water samples fall into the bicarbonate type.

Water Maturity

The maturity of geothermal water can be defined using the Na-K-Mg ternary diagram (Giggenbach, 1988), which classifies water based on its equilibrium state with rocks. Based on that diagram (Figure 3), all the spring samples fall into immature water category. This type of water contains high dissolved components originating from rock leaching or dilution by groundwater (Nicholson, 1993), as indicated by the high magnesium content in all the warm spring samples. Consequently, the water had not equilibrated with the reservoir rock, making them less reliable for geothermometry (Nicholson, 1993).

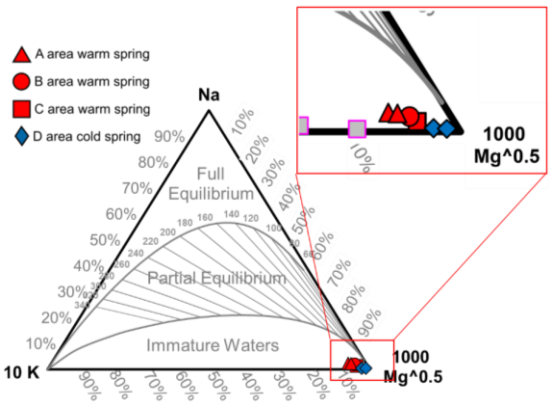

Figure 3. The Na-K-Mg diagram (Giggenbach, 1988, cited in Powell & Cumming, 2010) showing that all water samples fall into the immature water category

Fluid Origin

The δD vs δ18O isotope data were analyzed using diagram in Figure 4 to provide information about the fluid origin and the sub-surface processes. Based on the diagram, it can be interpreted that all the warm spring samples have a meteoric water origin as they were plotted along the Global Meteoric Water Line (GMWL: $\delta D‰ = 8\delta 18O + 10$; Craig, 1961) and the local meteoric water line (LMWL: $\delta D‰ = 7.23\ \delta 18O + 7.53$;Toulier et al., 2019), which were obtained from rainfall data in Kabupaten Pasuruan, approximately 46 km away from the research area. The meteoric origin of the warm springs is a result of the steam heating process and dilution by groundwater.

Fluid Processes

The Cl-Li-B diagram (Giggenbach, 1991) (Figure 5) was used to interpret the processes occurring within the fluids. Overall, all samples are divided into two main groups. The first group consists of warm springs in area C, plotted near the boron apex, while the second group comprises of warm springs in A and B areas, plotted near the chloride apex. The Cl vs. B diagram (Figure 6) can also be used to identify common reservoir (e.g., Glover, 1988, Arnórsson and Andrésdóttir, 1995 in Bégué et al., 2017). Based on this, all warm spring samples still were plotted in the same trend, indicating their origin from the same reservoir. The difference between groups on the ternary diagram (Figure 5) is due to the distinct processes occurring in both sample groups, notably higher dilution degree in the samples from area C.

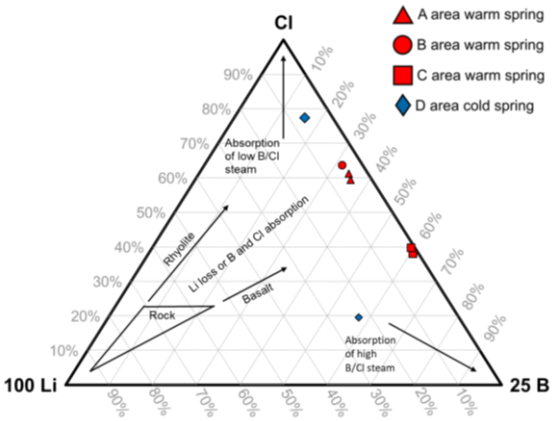

Figure 5. The Cl-Li-B diagram (Giggenbach, 1991, cited in Powell & Cumming, 2010) showing two group samples

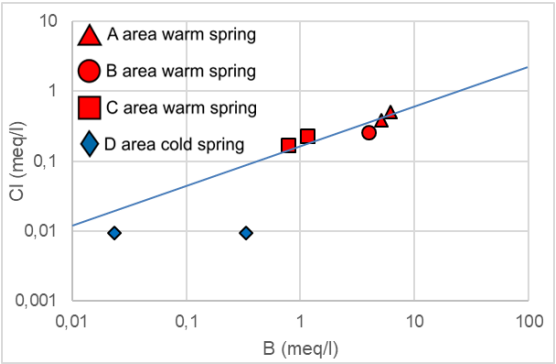

Figure 6. The Cl vs. B diagram showing trendline connecting the two sample groups and the lower concentrations of B and Cl in area C samples

Fluid Flow

Fluid flow was interpreted using various ratios of chemical constituents (Nicholson, 1993) in both water and gas samples, as shown in Table 4. In a high-relief geothermal systems

E-ISSN : 2579 – 3136

such as the YR field, geothermal manifestations like fumaroles, steaming ground, and sulphate-type hot springs generally formed near the upflow zone. Thus, the upflow zone of the system in interpreted to be at the peak of Mt. 7. Interpretation was also supported by the low value of CO_2/H_2S and CO_2/N_2 ratios observed in Mt. 7 solfatara. Gases with low values of these ratios were likely fed by steam, taking the most direct route to the surface. This was because H_2S gas tend to lost over time due to reactions with wall rocks and its transformation into steam condensate during migration. The outflow zone was interpreted to be in the west and northwest parts of Mt. 7, indicated by the presence of warm springs with high HCO_3/SO_4 ratios and low Cl/B, Na/K, and Cl/HCO_3 ratio values.

Table 4. Ratios of various water and gas geoindicators (Nicholson, 1993)

Sample	CO_2/H_2S	CO_2/NH_3	Cl/B	Na/K	HCO_3/SO_4	Cl/HCO_3
A1			41,5	3,9	6,0	0,19
A2			44,5	4,3	7,0	0,17
B			50,4	4,4	5,5	0,17
C1			16,7	3,4	8,8	0,06
C2			15,7	3,5	7,4	0,06
JV15-18	346,15	112,5				
JV15-18bis	3714,28	68,42				

Based on the chemical analysis that had been conducted, a hydrogeochemical model (Figure 7) was developed to better understand the fluid flow and processes in the geothermal system. The heat source of the YR geothermal system was interpreted to be located beneath the upflow zone in Mt. 7. This interpretation was based on the fact that the volcanic products of Mt. 7 are the most recent within the volcanic complex in research area, dating back to 200,000 years ago according to K-Ar dating (Hadi et al., 2010). Furthermore, the last eruption of this volcanic complex also took place at Mt. 7 in 1950 (ESDM, 2023).

The model of the YR geothermal field can be constructed using the liquid-dominated model proposed by Nicholson (1993) for high relief geothermal systems as an analogy. This is based on the field's morphology that situated in a high-elevation stratovolcano area, accompanied by the presence of fumaroles and advanced argillic alteration in the upflow areas, as well as the emergence of bicarbonate warm springs in the outflow areas on the mountain slopes.

The model showed that gas and vapor from degassing magma at depth reacted with reservoir liquid. As the pressure and temperature decreased, hot water and vapor underwent a boiling process and ascended as an upflow. Vapor with a high CO_2 content was then partially discharged as a Solfatara at the peak of Mt. 7, while the residual vapors cooled and generated superficial condensates. These condensates then flowed advectively downslope along the flank of Mt. 7. During their migration, the condensates underwent mixing process with shallow groundwater and reacted with wall rocks, resulting in the production of diluted, immature bicarbonate water at A, B, and C areas in the western and northwestern flank of Mt. 7.

CONCLUSION

All spring samples in the research area were classified as bicarbonate type immature water resulting from steam heating process. Thus, the water samples had not reached equilibrium and cannot adequately reflect the reservoir condition. The characteristics differences between area C warm springs and area A and B warm springs were due to distinct processes, where the warm water in area C underwent more intensive dilution, resulting in lower chloride content.

The upflow zone was interpreted to be at the peak of Mount 7, while the outflow zone was interpreted to be in A, B, and C areas. High-temperature vapor and gas rose within the upflow zone then underwent condensation and flowed advectively downslope. The fluid also underwent reactions with side rocks, and mixed with meteoric water during their flow. The fluid then emerged in the outflow zone towards the west and northwest of Mount 7 as low-temperature neutral pH warm springs.

ACKNOWLEDGEMENT

The authors are gratefully acknowledging PT. Geo Dipa Energi (Persero) which has provided the geochemical data as well as the opportunity to conduct research related to the hydrogeochemical model of YR field.

REFERENCES

Bogie, I., Lawless, J., Rychagov, S., & Belousov, V. (2005). Magmatic-related hydrothermal systems: classification of the types of geo- thermal systems and their ore mineralization. *Proceedings of Geoconference*.

ESDM. (2023). *Gunung Arjuno Welirang*.

E-ISSN : 2579 – 3136

Giggenbach, W. F. (1988). Geothermal solute equilibria. Derivation of Na-K-Mg-Ca geoindicators. *Geochimica et Cosmochimica Acta*, *52*(12), 2749–2765. https://doi.org/10.1016/0016-7037(88)90143-3

Giggenbach, W. F. (1991). *Chemical Techniques in Geothermal Exploration, Application Of Geochemistry In Geothermal Reservoir Development*. 119–142.

Hadi, M. N., Kusnadi, D., & Rezky, Y. (2010). PENYELIDIKAN TERPADU GEOLOGI DAN GEOKIMIA DAERAH PANAS BUMI ARJUNO - WELIRANG, KABUPATEN MOJOKERTO DAN MALANG, PROVINSI JAWA TIMUR. *Prosiding Hasil Kegiatan Pusat Sumber Daya Geologi*, 405–416.

Hutchings, S. J., & Mooney, W. D. (2021). The Seismicity of Indonesia and Tectonic Implications. *Geochemistry, Geophysics, Geosystems*, *22*(9). https://doi.org/10.1029/2021GC009812

Inguaggiato, S., Mazzini, A., Vita, F., & Sciarra, A. (2018). The Arjuno-Welirang volcanic complex and the connected Lusi system: Geochemical evidences. *Marine and Petroleum Geology*, *90*, 67–76. https://doi.org/10.1016/j.marpetgeo.2017.10.015

Nicholson, K. (1993). *Geothermal Fluids: Chemistry and Exploration Techniques*. Springer Berlin Heidelberg. https://doi.org/10.1007/978-3-642-77844-5

PT. Geo Dipa Energi. (2018). *Internal report of fluid analysis (unpublished)*.

Rahayudin, Y., Kashiwaya, K., Tada, Y., Iskandar, I., Koike, K., Atmaja, R. W., & Herdianita, N. R. (2020). On the origin and evolution of geothermal fluids in the Patuha Geothermal Field, Indonesia based on geochemical and stable isotope data. *Applied Geochemistry*, *114*, 104530. https://doi.org/10.1016/j.apgeochem.2020.104530

Simkin, T. L., & Siebert, L. (1994). *Volcanoes of the World*. Geoscience Press.

Stober, I., & Bucher, K. (2013). *Geothermal Energy*. Springer Berlin Heidelberg. https://doi.org/10.1007/978-3-642-13352-7

Toulier, A., Baud, B., de Montety, V., Lachassagne, P., Leonardi, V., Pistre, S., Dautria, J.-M., Hendrayana, H., Miftakhul Fajar, M. H., Satrya Muhammad, A., Beon, O., & Jourde, H. (2019). Multidisciplinary study with quantitative analysis of isotopic data for the assessment of recharge and functioning of volcanic aquifers: Case of Bromo-Tengger volcano, Indonesia. *Journal of Hydrology: Regional Studies*, *26*, 100634. https://doi.org/10.1016/j.ejrh.2019.100634

E-ISSN : 2579 – 3136

Table 1. Physical characteristics of each manifestation in study area(PT. Geo Dipa Energi, 2018)

Sample	T (°C)	pH	EC (µs)	TDS (mg/kg)	Description
A1	54,8	6,41	3,4	2340	No sulphur smell, has iron oxide deposit and minor travertine
A2	41,2	6,14	3,09	2050	No sulphur smell, has iron oxide deposit
B	29,4	6,19	1086	1650	No sulphur smell, has iron oxide deposit
C1	52,5	6,44	1662	1290	No sulphur smell
C2	44,2	6,44	1275	854	No sulphur smell
D1	18,2	6,52	134,5	102	No sulphur smell, has iron oxide deposit
D2	18,4	7	455,7	295	No sulphur smell, has iron oxide deposit

Table 2. Chemical constituents of the water samples in the study area (PT. Geo Dipa Energi, 2018)

Sample	Na	K	Ca	Mg	Cl	SO_4	HCO_3	B
	mg/kg							
A1	255	64,7	143	110	221	192	1150	5,32
A2	219	51,1	131	95,1	182	153	1070	4,09
B	167	38,2	96,9	85,4	141	150	828	2,8
C1	110	32,8	63,6	79,8	41,5	86,1	754	2,48
C2	77,7	22,2	49,4	37,4	28,1	61,8	457	1,79
D1	3,83	2,45	7,56	1,04	0,849	2,79	35,3	0,1
D2	9,52	3,57	36,3	9,82	11,9	59,1	85,5	0,1

Table 3. Chemical constituents of the gas manifestations in the study area (Inguaggiato et al., 2018)

Sample	T	H_2O	CO_2	HF	HCl	H_2S	SO_2	He	H_2	O_2	N_2	CO	CH_4
	(°C)				%Vol								
JV15-18	220	92,8	4,5	bdl	1.9E-01	1.3E-02	2.50	3.8E-05	4.0E-02	5.0E-05	2.4E-02	5.5E-06	3.0E-06
JV15-18bis	115	96,7	2,6	bdl	2.7E-02	7.0E-04	0.68	3.6E-05	3.8E-02	2.1E-05	2.0E-02	1.7E-06	5.5E-06

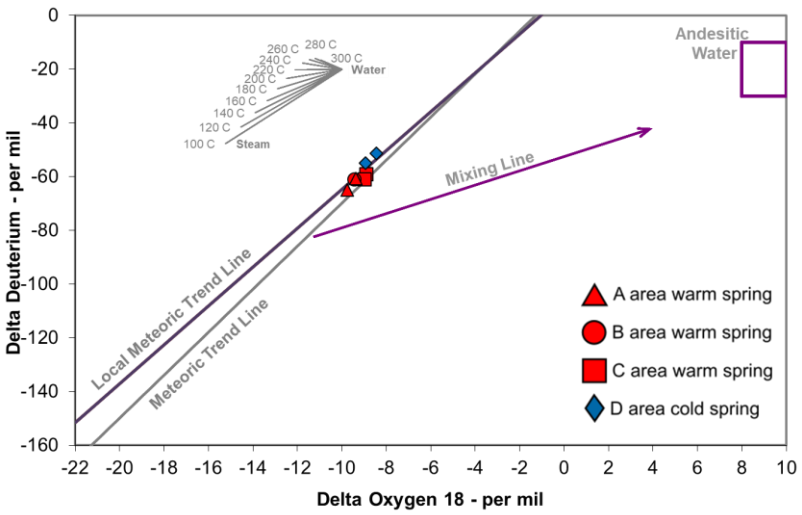

Figure 4. δD - δ^{18}O isotope diagram showing meteoric origin for all warm spring water samples

E-ISSN : 2579 – 3136

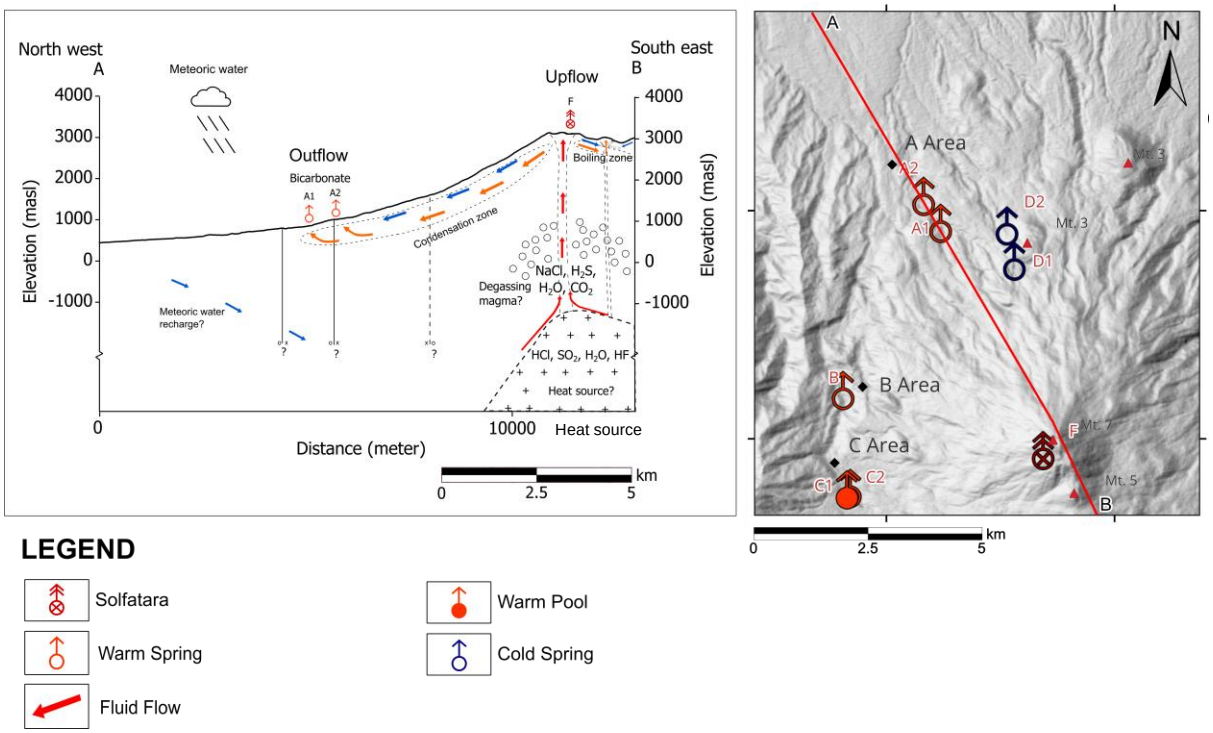

Figure 7. Hydrogeochemical model of study area, showing fluid flow and processes in the geothermal system

E-ISSN : 2579 – 3136